Nb-doped variants of high surface aluminium fluoride: a very strong bi-acidic solid catalyst†‡

Clara Patricia Marshall,[a,b] Gudrun Scholz,[a] Thomas Braun [ID] *[a] and Erhard Kemnitz [ID] *[a]

A niobium doped high surface aluminium fluoride (*HS*-AlF₃) catalyst was prepared, using an approach in which niobium doped aluminium hydroxide fluoride obtained *via* reaction of aqueous HF with the respective metal alkoxides in isopropanol is further fluorinated under flow of CHClF₂ at 200 °C. A comparable procedure was used to synthesize a Nb-free variant for comparison. Both catalysts exhibit very strong Lewis acidic surface sites which are capable to activate strong carbon–halogen bonds at room temperature, just as the classical high-surface AlF₃ (*HS*-AlF₃), obtained by reacting aluminium isopropoxide with anhydrous HF, does. The catalysts were characterized by elemental analysis, P-XRD, MAS NMR spectroscopy, N₂ adsorption, NH₃-TPD, and pyridine photoacoustic FT-IR spectroscopy. In contrast to previously reported niobium doped *HS*-AlF₃, which was prepared using anhydrous HF, the doped catalyst obtained *via* this aqueous HF-route shows excellent performance both in the isomerization of 1,2-dibromohexafluoropropane, a reaction that occurs only in the presence of the strongest Lewis acids, and in the cyclization of citronellal to isopulegol, a reaction which requires both, Lewis and Brønsted acid sites.

Introduction

Metal fluorides can be regarded as an interesting alternative to their metal oxide counterparts. Fluorine has a higher electronegativity than oxygen, and therefore, metal fluorides should usually exhibit a higher Lewis acidity than the respective oxides. Moreover, metal fluorides are thermally and chemically stable as well.[1,2] More specifically, aluminium fluoride-based catalysts have attracted attention since decades, in particular after the development of the fluorolytic sol–gel synthesis in 2003, where an amorphous aluminium fluoride phase prepared by a two-step fluorolytic sol–gel synthesis was developed.[3] The benefit of the mesoporous *HS*-AlF₃ phase obtained that way is its high-surface area, as determined by BET experiments, exhibiting extremely strong Lewis acidic surface sites. For comparison, the metastable β-AlF₃ phase, classically the most active AlF₃ polymorph, has a surface area ten times lower exhibiting macroporosity and just medium strong Lewis surface sites.[2]

The fluorolytic sol–gel approach for metal fluorides allows for flexibility in the synthesis procedure, since many parameters can be changed independently, such as concentration, temperature, metal precursor source, solvent, *etc.*[4,5] The presence of water plays a crucial role, since hydrolysis of the metal–alkoxide bond of the aluminium alkoxide precursor may be an issue if water is added to the reaction mixture, thus creating additional surface Brønsted sites. Consequently, in the past years, several studies have been published where the effect of water addition was studied for metal fluorides prepared by sol–gel chemistry or other methods, such as mechanochemistry.[6–9] The general consensus is that if aqueous HF is used as a source for fluorination, or water is added to the reaction mixture, the final product will be a metal hydroxide fluoride. With respect to their acidic sites, these solids possess both acid types, Lewis and Brønsted, and their relative amount can be adjusted *via* the F/OH ratio that strongly depends on the amount of water added.[10,11]

Metal hydroxide fluorides obtained this way are, unless thermally treated, X-ray amorphous materials, and possess strong acid sites as determined by ammonia TPD.[9,12] They also show exciting catalytic properties. Thus, Agirrezabal-Telleria *et al.* used a partially hydroxylated magnesium fluoride for the dehydration of xylose to furfural, and Hemmann and Teinz reported on the cyclization of citronellal to isopulegol with high selectivity at different aluminium hydroxide fluoride phases.[13–15] Although aluminium hydroxide fluorides represent a very interesting new class of bi-acidic solid catalysts,

[a]Department of Chemistry, Humboldt-Universität zu Berlin, Brook-Taylor-Straße 2, D-12489 Berlin, Germany. E-mail: thomas.braun@cms.hu-berlin.de, erhard.kemnitz@chemie.hu-berlin.de

[b]School of Analytical Sciences Adlershof (SALSA), Humboldt-Universität zu Berlin, Unter den Linden 6, 10099 Berlin, Germany

† Dedicated to Dr Johannes Eicher on the occasion of his 60th birthday.
‡ Electronic supplementary information (ESI) available. See DOI: 10.1039/c9dt00831d
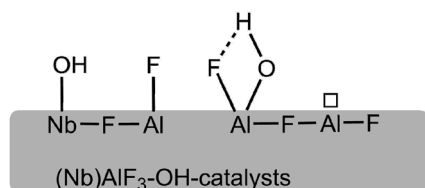
Fig. 1 Pictorial description of the catalysts surface.

no AlF_3-phase nor any other metal fluoride phase has been reported so far that exhibits very strong Lewis surface sites when Brønsted sites co-exist in a near neighbourhood. It is assumed that Al–OH surface sites cause the formation of Al–O–H···F–Al hydrogen bridges, resulting in a rearrangement at the surface, which in turn blocks the very strong Al-Lewis sites on the surface (see Fig. 1).[16]

We recently reported on the preparation of Nb-doped *HS*-AlF_3 by reacting alkoxide precursors with anhydrous HF in isopropanol. The presence of Nb unfortunately caused a decrease in the Lewis acidity compared to the undoped material, as indicated by the catalytic performance of the materials, however Brønsted acid sites were also observed at the catalyst.[17] The activity in the isomerization of 1,2-dibromohexafluoropropane, a reaction that only occurs at very strong Lewis acids like SbF_5, aluminium chlorofluoride, or *HS*-AlF_3, was significantly lower for Nb-doped *HS*-AlF_3 than undoped *HS*-AlF_3 (15 to 99%).

Based on these results, in this paper we present a new synthetic approach by using HF_{aq} to access a Nb-doped *HS*-AlF_3 that contains Brønsted-sites besides very strong Lewis sites and is able to perform the above-mentioned isomerization reaction of 1,2-dibromohexafluoropropane with nearly 100% conversion. In this approach, we make use of the fact that the thermodynamic stability of the Nb–O bond in comparison to the Nb–F bond is significantly more pronounced than the Al–O to Al–F bond. The preparation involves the intermediate formation of aluminium hydroxide fluoride phases as precursors, by using aqueous HF as fluorinating agent instead of alcoholic solutions of anhydrous HF. The aluminium hydroxide fluoride phase and the Nb-doped variation were both post-fluorinated; all four materials were thoroughly characterized, in particular by MAS NMR spectroscopy and tested in specific catalytic reactions.

Experimental details

Catalyst preparation

All the reactions, unless otherwise stated, were performed under standard Schlenk conditions. The four catalysts intro-

duced in this work were prepared as depicted in Fig. 2, using a similar procedure. Along the paper, the following nomenclature will be used: AlF_3-OH refers to the xerogel obtained by drying the gel that has been formed after aqueous HF addition to aluminium isopropoxide; AlF_3-OH_{post} refers to the solid obtained after postfluorination of AlF_3-OH. Nb-AlF_3-OH and Nb-AlF_3-OH_{post} are the corresponding doped variants, prepared with the addition of 5% mol of Nb to Al.

Aluminium isopropoxide (Sigma Aldrich, 98%) was dissolved in dry isopropanol –previously distilled under molecular sieves– and heated under reflux for 1 hour. After cooling down the mixture, a solution of aqueous HF (39.32 M, 78%) was added, in stoichiometric conditions. A transparent gel was formed, which was left to age for 24 hours before removal of the solvent under vacuum. The xerogel obtained was then stored in a glovebox (AlF_3-OH). For the preparation of AlF_3-OH_{post}, AlF_3-OH was treated further in a post-fluorination step. For this, the sample was treated at 240 °C under a flow of N_2 and $CHClF_2$ (ratio of 4 : 1) in a Ni reactor. In the case of the Nb-doped sample, the desired amount (5% mol of Nb to Al) of niobium ethoxide (Strem Chemicals, 99.9%) was added with a syringe to the aluminium isopropoxide in isopropanol and left to dissolve. Aqueous HF was added stoichiometrically for full fluorination of both metal sources and the solvent was removed to obtain a xerogel (Nb-AlF_3-OH). A post-fluorination treatment with $CHClF_2$ was also performed, in this case the full catalytic Lewis activity was achieved already at 200 °C, producing the catalyst Nb-AlF_3-OH_{post}.

For comparison along this report, *HS*-AlF_3 and Nb5 (*HS*-AlF_3 with 5% mol of Nb – in this report herein named as Nb-AlF_{3-post}) were prepared following reported procedures.[3,17] The main difference between these two catalysts (*HS*-AlF_3 and Nb5) and the ones presented here is the HF source used for fluorination: anhydrous HF dissolved in isopropanol (HF_{iPrOH}) instead of aqueous HF (HF_{aq}, 39.32 M, 78%) which was used here.

NH_3-TPD

To determine the number and strength of the acid sites, the catalysts were characterized by temperature programmed desorption (TPD) using ammonia as a probe molecule. For this, 0.2 g of the catalyst were added in a quartz flow reactor and heated at 300 °C under nitrogen flow for 1 hour. After cooling down until 120 °C, ammonia was adsorbed on the surface, and the excess removed by nitrogen flow for 1 h. The desorption was performed using a heating rate of 10 °C min^{-1} up to 500 °C, kept at 500 °C until no more NH_3 is desorbed. The process was monitored by FT-IR spectroscopy (FT-IR System,
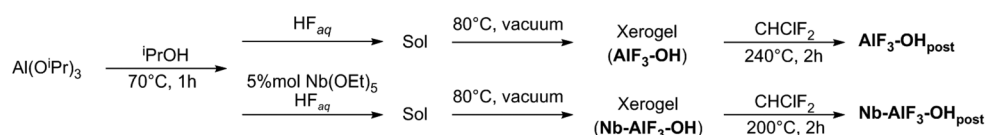

Fig. 2 Scheme of catalysts preparation, with the nomenclature used in this work.

PerkinElmer) following the band at 930 cm^{-1}. The total amount of ammonia desorbed was quantified by back-titration with a sodium hydroxide solution after treatment with excess sulfuric acid.

Pyridine-FT-IR-PAS

To identify the presence of Lewis and/or Brønsted acid sites in the catalyst, pyridine was used as a probe molecule in a FT-IR photoacoustic spectroscopy (PAS) experiment. For this, the sample was loaded with pyridine at 150 °C and left under N_2 flow to remove physisorbed species. Afterwards, it was transferred into the photoacoustic cell (MTEC 200) and the respective IR spectrum was recorded at room temperature using a FTIR system 2000, PerkinElmer. Background spectra, without loading of probe molecule, were additionally measured for each sample.

^1H, ^{19}F and ^{27}Al MAS NMR spectroscopy

Solid-state MAS (magic angle spinning) nuclear magnetic resonance spectra were recorded on a Bruker AVANCE 400 spectrometer at room temperature. The samples were filled in 2.5 mm rotors in a glovebox to avoid contact with moisture. The spectra were recorded using a rotation frequency of 20 kHz (for ^{19}F, ^1H and ^{27}Al) or 25 kHz (for ^{19}F). All ^{19}F spectra were measured using a $\pi/2$ pulse length of 4.2 μs, a spectrum width of 400 kHz, a recycle delay of 5 s and an accumulation number of 32. All ^1H spectra were measured using a $\pi/2$ pulse length of 3.8 μs, a spectrum width of 400 kHz, a recycle delay of 5 s and an accumulation number of 256. Recycle delays longer than 5 s were tested to ensure the completeness of the signals and to inspect their spin–lattice relaxation behaviour. Existent background signals were suppressed with the application of a phase-cycled depth pulse sequence according to Cory and Ritchey.[18] The rotor-synchronized ^{19}F and ^1H spin-echo experiments were registered with a recycle delay of 5 s, an accumulation number of 1024 for ^{19}F and of 256 for ^1H respectively, and a dipolar evolution time of 0.5 ms. ^{27}Al MAS NMR (I = 5/2) spectra were recorded with an excitation pulse duration of 1 μs, and an accumulation number of 512. ^1H chemical shifts are referred to TMS, and adamantane was used as a secondary standard for calibration. ^{19}F chemical shifts are referred to δ = 0 ppm of $CFCl_3$, ^{27}Al chemical shifts are given with respect to δ = 0 ppm of 1 M $AlCl_3$ solution. For both nuclei, α-AlF_3 was used as a secondary standard for calibration.

Elemental analysis

Carbon, hydrogen and nitrogen content of the samples were determined by elemental analysis by means of a EURO EA device (HEKATech GmbH). The samples were prepared under inert atmosphere during handling.

P-XRD

Powder-X-ray-diffractograms were recorded on an XRD-3003-TT diffractometer (Seiffert & Co., Freiberg), with Cu-Kα as radiation source (*l* = 1.542 Å). The samples were prepared in the glovebox and covered with Kapton® film during the whole measurement.

Surface area determination by N_2 adsorption

Surface area (using the BET model) and porosity (assessed with the BJH model) were measured using nitrogen sorption at −196 °C. An ASAP 2010 (Micromeritics Instrument Corp., USA) instrument was used, and the samples were degassed for 6 h either at 50 °C (for the precursors) or at 200 °C (for the post-fluorinated solids).

Dismutation of $CHClF_2$ (Fig. 3a)

This test reaction can be performed *in situ* during the post-fluorination step and followed at different temperatures.[3,19] At room temperature, only strong Lewis acids can show full conversion. The flow reactor used for the final synthetic step was built with a septum in the outlet from which samples could be taken and measured. A GC-2010 (Shimadzu) equipped with an HP-1 capillary column and an FID detector, with nitrogen as carrier gas, was used to follow the reaction. Conversions were calculated relatively from the ratio of $CHClF_2$ to the different products (CHF_3, $CHCl_3$, $CHCl_2F$).

Isomerization of 1,2-dibromohexafluoropropane to 2,2-dibromohexafluoropropane (Fig. 3b)

To 25 mg of the catalyst, 250 μL of the substrate (Alfa Aesar, 98%) were added, and the mixture was left to react for 2 hours at room temperature. Water was added to stop the reaction, and $CDCl_3$ to dissolve the product: the organic phase was separated and subjected to ^{19}F NMR analysis. Conversions were
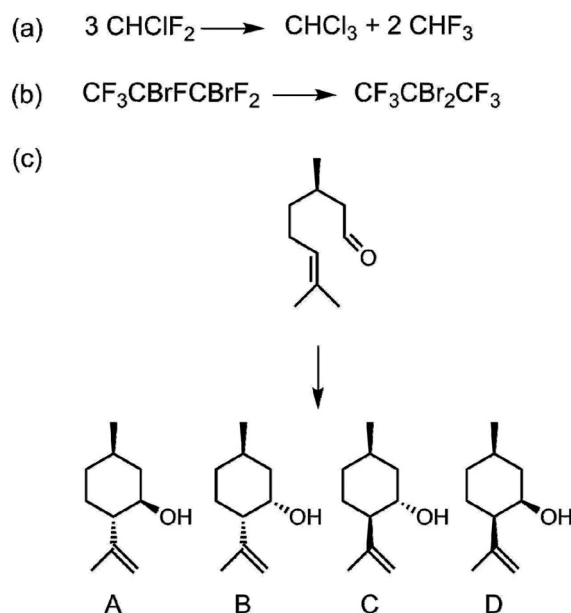
Fig. 3 Scheme of catalytic reactions tested: (a) dismutation of $CHClF_2$, (b) isomerization of 1,2-dibromohexafluoropropane and (c) cyclization of citronellal to isopulegol (A), neo-isopulegol (B), iso-isopulegol (C) and neoiso-isopulegol (D).

calculated *via* integration of the signals of substrate and product in the spectra.

Cyclization of citronellal (Fig. 3c)

Inside a glovebox, a Teflon tube was filled with 25 mg of the catalyst and sealed with a rubber septum. The tube was inserted in an Eppendorf Thermomixer comfort, and toluene (3 mL), citronellal (0.3 mL) and undecane (0.15 mL) as an internal standard were added. The mixture was stirred 6 h at 80 °C at 600 rpm, then cooled down in an ice bath. The catalyst was filtered off and the respective solution was investigated by GC-FID; retention times were compared to those reported.[15]

Results and discussion

Catalyst synthesis

In this work, the original synthesis of *HS*-AlF$_3$ was modified using an aqueous solution of HF instead of anhydrous HF to fluorinate aluminium isopropoxide, and simultaneously niobium ethoxide in the case of the Nb-doped *HS*-AlF$_3$. Fig. 2 depicts the synthesis pathways, which are analogous to the ones already described.[17]

AlF$_3$-OH and Nb-AlF$_3$-AlOH were prepared by the addition of aqueous HF to the solution of aluminium isopropoxide and niobium ethoxide in isopropanol. A transparent gel was obtained, comparable to the ones obtained *via* the water-free route mentioned beforehand.[17] After solvent removal, xerogels were obtained in both cases as fine white powders. To characterize them, elemental analysis and P-XRD were carried out: both AlF$_3$-OH and Nb-AlF$_3$-AlOH are amorphous, and possess low carbon content (8.2% and 10.3% respectively, see Table S1‡) when compared to phases obtained from reaction with a-HF$_{iPrOH}$. Since there are still organic species in the materials, according to elemental analysis, these two catalysts should more correctly be considered as aluminium hydroxo-alkoxo-fluorides (Al(OR)$_{3-x}$(OH)$_y$F$_z$).

If AlF$_3$-OH and Nb-AlF$_3$-OH are compared to the xerogel precursor of *HS*-AlF$_3$, a remarkable difference arises. Although all three compounds are X-ray amorphous, the carbon content for the *HS*-AlF$_3$ xerogel prepared with a-HF$_{iPrOH}$ is with *ca.* 30% significantly higher. Surprisingly, using aqueous HF solutions for fluorination resulted in drastically lower carbon contents for AlF$_3$-OH and Nb-AlF$_3$-OH. It is evident from these elemental analysis results that aqueous HF causes a higher degree of conversion on the alkoxide, compared to a-HF$_{iPrOH}$. The number of unreacted alkoxide groups in AlF$_3$-OH and Nb-AlF$_3$-OH is lower, due to an extended dissociation of HF resulting possibly in increased reactivity.

The lower amount of carbon in AlF$_3$-OH and Nb-AlF$_3$-OH presents the first advantage over the sample obtained from the synthesis of *HS*-AlF$_3$ using a-HF$_{iPrOH}$. It is known, that in the course of postfluorination of the (Al(OR)$_{3-x}$(OH)$_y$F$_z$) phases extremely strong Lewis sites are formed, which – if the post-fluorination with a chlorofluorocarbon gas stream is not carefully performed – can be accompanied by significant coke for-

mation resulting in a blocking of very strong Lewis surface sites.[19,20] However, a higher degree of fluorination already during the sol–gel synthesis can suppress the problem of coke formation.

To prepare AlF$_3$-OH$_{post}$ and Nb-AlF$_3$-OH$_{post}$, the corresponding xerogels AlF$_3$-OH and Nb-AlF$_3$-OH were subjected to a post-fluorination step. The combination of thermal treatment and reaction with a fluorinating agent such as CHClF$_2$ permits the preparation of fully fluorinated solids. To probe the completeness of this postfluorination step, the full conversion of the fluorinating agent in the dismutation reaction was used as a positive control. These post-fluorinated catalysts AlF$_3$-OH$_{post}$ and Nb-AlF$_3$-OH$_{post}$ are brown granular solids, and as their xerogel counterparts, amorphous based on P-XRD. Considering the carbon content, this is significantly reduced in the solids after the postfluorination step and is as little as 2.6% and 0.9% for AlF$_3$-OH$_{post}$ and Nb-AlF$_3$-OH$_{post}$, respectively (see Table S1‡). However, since *HS*-AlF$_3$ obtained from the reaction of Al(O^{i}Pr)$_3$ with a-HF$_{iPrOH}$ contains 1.6% carbon after postfluorination, the use of HF$_{aq.}$ as a fluorinating source does not have an apparently significant effect on the amount of the remaining organic content in the final post-fluorinated material.

Regarding the described synthesis routes, two comments should be pointed out. Firstly, just as the original route to Nb-doped *HS*-AlF$_3$, the inclusion of Nb centres generates enough Lewis acid sites in the catalyst to achieve full catalytic activity in the dismutation of CHClF$_2$ during post-fluorination already at 200 °C. A higher temperature to enable full conversion of chlorodifluoromethane is not required, as in the case of AlF$_3$-OH$_{post}$ or *HS*-AlF$_3$. Secondly, the effect of using aqueous HF obviously causes to some part not only a higher degree of fluorination but also a higher extent of hydrolysis. This issue was further studied with several characterization methods which are presented in the next sections.

The Nb-AlF$_3$-OH$_{post}$ catalyst behaves very similar as *HS*-AlF$_3$, it is stable for a long time if stored in N$_2$ atmosphere, but takes up water if handled at air. Consequently, the very strong surface Lewis sites are blocked resulting in reduced catalytic activity. However, as known for *HS*-AlF$_3$, full catalytic activity can be recovered by heating the Nb-AlF$_3$-OH$_{post}$ catalyst in a dry nitrogen flow up to *ca.* 300 °C (see ref. 20 and 21).

N$_2$ adsorption experiments

The adsorption of N$_2$ at −196 °C provides crucial morphological information for any heterogeneous catalyst: surface area, pore size and pore volume. This set of information is summarized in Table 1 for the different catalysts studied. The corresponding isotherms are depicted in Fig. 4, for both AlF$_3$-OH$_{post}$/AlF$_3$-OH (left) and Nb-AlF$_3$-OH$_{post}$/Nb-AlF$_3$-OH(right). All the catalysts exhibit high BET surface areas, the highest in particular for both AlF$_3$-OH and Nb-AlF$_3$-OH (Table 1, entries 4 and 6), with values of *ca.* 460 m^2 g^{-1}. The effect of the postfluorination step results in a decrease of the surface area, and an increase of both, pore size and pore volume, after the treat-

Table 1 Summary of characterization

Entry	Catalyst	BET surface area [m² g⁻¹]	Pore size[a] [Å]	Pore volume [cm³ g⁻¹]	Acid sites[b] [μmol g⁻¹]	Acid sites per surface area [μmol m⁻²]
1	*HS*-AlF₃[c]	240	69	0.50	1510	6.29
2	Nb-AlF₃₋post[c]	251	50	0.37	1303	5.19
3	AlF₃-OHpost	255	165	1.19	1968	7.71
4	AlF₃-OH	467	73	0.93	1491	3.19
5	Nb-AlF₃-OHpost	267	72	0.59	1843	6.90
6	Nb-AlF₃-OH	460	40	0.41	1810	3.93

[a] Average pore size, as calculated from BJH model (4 A V⁻¹). [b] Determined by NH₃-TPD. [c] From ref. 17.

ment at 200 °C (for Nb-AlF₃-OHpost) or 240 °C (for AlF₃-OHpost) with CHClF₂.

The isotherms can be classified as type IV according to IUPAC, typical for mesoporous solids.[22] Nb-AlF₃-OH has a different shape compared to the others, due to a broader distribution in pore sizes (see Fig. S1‡). All four isotherms show differences with respect to adsorption and desorption and such hysteresis can be identified as type H3 and, in the case of Nb-AlF₃-OH, type H4. They correspond to aggregates of particles with slit-shaped pores, which have a non-uniform (for H3) or uniform (for H4) shape and size.[23]

Pore size distributions are shown in Fig. S1,‡ applying the BJH model, for all four catalysts. The undoped ones, AlF₃-OHpost and AlF₃-OH, have quite similar distributions, with pore widths in the mesopore region. Particularly, AlF₃-OH has also a micropore contribution, which under the experimental conditions used here cannot be determined, and pore sizes should be below 20 Å. The Nb-doped catalysts, on the other hand, show different pore size distribution. The post-fluorinated catalyst, Nb-AlF₃-OHpost, exhibits only mesopores, whereas Nb-AlF₃-OH possesses a mixture of mesopores and micropores, as seen from the broad shape of the distribution.
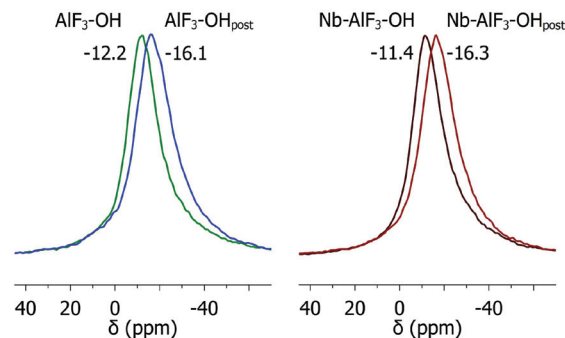

Fig. 5 ^{27}Al MAS NMR spectra for AlF₃-OH and AlF₃-OHpost (left) and Nb-AlF₃-OH and Nb-AlF₃-OHpost (right) measured at 20 kHz rotation frequency, ns = 512; the chemical shifts of the signal maxima are indicated in the figure.

MAS NMR spectroscopy

MAS NMR spectroscopy is an important analytical tool for these catalysts to gain information about local environments of such XRD amorphous solids. Aluminium hydroxide fluoride phases possess three NMR active nuclei which can be studied: ^{1}H, ^{19}F and ^{27}Al. Several experiments were performed and the obtained results are presented in Fig. 5 (^{27}Al MAS NMR spectra), Fig. 6 (^{19}F MAS NMR spectra), Fig. 7 (^{19}F spin-echo-rotor-synchronized spectra) and Fig. 8 (^{1}H spin-echo-rotor-synchronized spectra and ^{1}H MAS NMR spectra).

^{27}Al MAS NMR spectroscopy. The ^{27}Al MAS NMR spectra show a broad peak for all samples at chemical shifts varying from −11 to −16 ppm (Fig. 5). These signals are typical for aluminium in a distorted octahedral F⁻ environment and are also commonly found for *HS*-AlF₃. The asymmetric high-field decay is related to the distribution of varying bond lengths and bond angles existing in the solid.

König *et al.*[24] elaborated a trend analysis for ^{27}Al NMR chemical shifts for several crystalline species of aluminium (hydroxide) fluorides AlF$_x$(OH)$_{3−x}$, considering crystalline com-

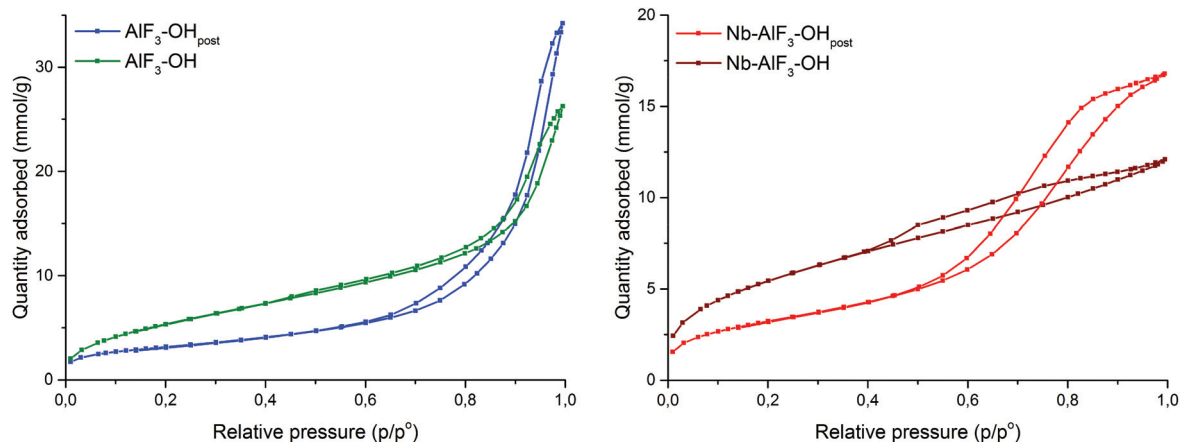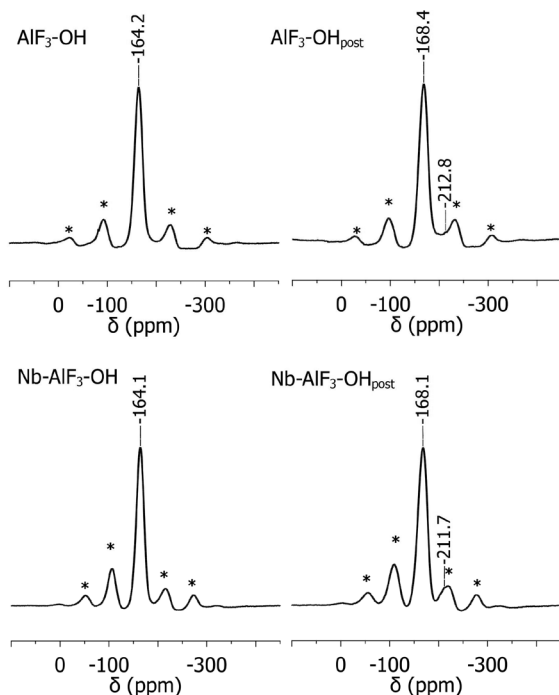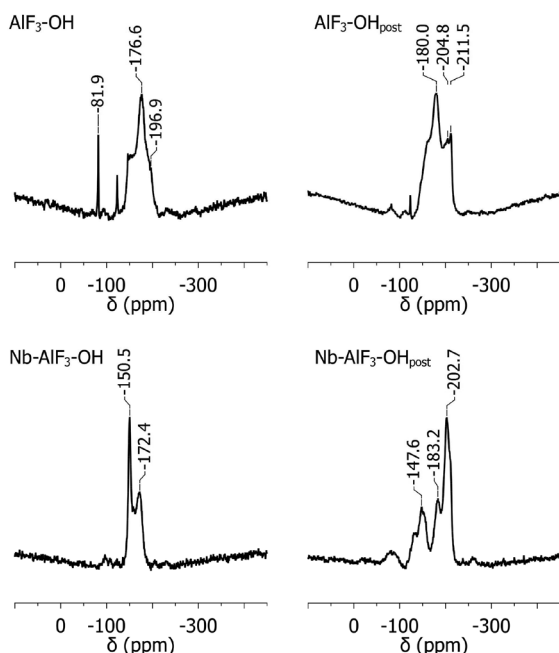**Fig. 4** N₂ adsorption and desorption isotherms at −196 °C for AlF₃-OH and AlF₃-OHpost (left) and Nb-AlF₃-OH and Nb-AlF₃-OHpost (right).

Fig. 6 ^{19}F MAS NMR spectra for Nb-AlF$_3$-OH (down-left) and Nb-AlF$_3$-OH$_{post}$ (down-right), measured at 20 kHz rotation frequency, ns = 32 and for AlF$_3$-OH (up-left, 20 kHz) and AlF$_3$-OH$_{post}$ (up-right), measured at 25 kHz, ns = 32 (*: spinning side bands).

Fig. 7 ^{19}F MAS spin-echo-rotor-synchronized NMR spectra for Nb-AlF$_3$-OH (down-left) and Nb-AlF$_3$-OH$_{post}$ (down-right), measured at 20 kHz rotation frequency, a dipolar evolution time of 0.5 ms, ns = 1024; and for AlF$_3$-OH (up-left, 20 kHz) and AlF$_3$-OH$_{post}$ (up-right, ν_{rot} = 25 kHz), dipolar evolution time: 0.5 ms, ns = 1024.

pounds formed by different but AlF$_x$O$_{(x-y)/2}$ polyhedral units of known structure.[7,8] Amorphous compounds like aluminium isopropoxide fluoride can be interpreted on using the same analysis since they also consist of distorted octahedral AlF$_x$(OX)$_{x-6}$-units (X being an H or alkyl moiety).[25] Based on these studies, a ^{27}Al signal at about −11 ppm, as observed here for AlF$_3$-OH and Nb-AlF$_3$-OH, can be assigned to aluminium atoms in a coordination sphere of the type AlF$_5$O, whereas the value of −16 ppm present in the spectra of post-fluorinated materials, can be assigned to AlF$_6$ species. The origin of the AlF$_5$O species cannot be clearly assigned since they could correspond either to hydroxide or isopropoxide moieties co-ordinated to aluminium.[25]

^{19}F MAS NMR spectroscopy. The ^{19}F MAS spectra (Fig. 6) exhibit only one broad signal, between −164 ppm and −168 ppm, which corresponds to fluorine atoms in a bridging position between two aluminium centres, and bonded to aluminium in an octahedral environment. Due to the shape and widths of these signals, it can be assumed that many different fluorine species are present. In the case of AlF$_3$-OH$_{post}$ and Nb-AlF$_3$-OH$_{post}$, a small signal was additionally observed at −210 ppm, which is characteristic for terminal fluorine atoms bound to sub-coordinated surface aluminium sites.[26]

In addition, and to better comprehend these signals, spin-echo-rotor-synchronized experiments were carried out. The results for the catalysts studied here are presented in Fig. 7. The rotor-synchronized spin-echo ^{19}F MAS NMR spectrum of the Nb-AlF$_3$-OH phase depicts two signals, one at −150 ppm and another one with a lower intensity at −172 ppm (Fig. 7, left, bottom-down). Both signals are covered in the ^{19}F MAS NMR spectrum (Fig. 6), and can be assigned according to a ^{19}F NMR chemical shift trend analysis to AlF$_x$O$_{6-x}$ building blocks as reported in the literature.[27] It suggests that the smaller the number of fluorine atoms at an aluminium centre is, the stronger is the low-field shift of the ^{19}F NMR signal. Therefore, the signal at −150 ppm can be interpreted resulting from an AlF$_4$O$_2$ unit, and the one at −172 ppm from an AlF$_6$ species. The spin-echo spectrum of AlF$_3$-OH (Fig. 7, left-up) exhibits two signals, at −176 ppm and at −196 ppm. The latter corresponds to a terminal fluorine species, however, it is not intense. The signal at −176 ppm can be assigned to an AlF$_6$ unit and is also present in the corresponding post-fluorinated catalyst. Besides these two, an additional sharp signal appears at −81 ppm: this signal corresponds to a –CF$_3$ moiety, and might belong to impurities from fluorinated grease used in the synthesis.

Both spectra of AlF$_3$-OH$_{post}$ and Nb-AlF$_3$-OH$_{post}$ exhibit sharp signals between −202 and −211 ppm, consistent with the presence of terminal non-bridging fluorine atoms in these catalysts, usually being a clear hint for very strong Lewis acidity of the solid AlF$_3$-phase.[2] Thus, the addition of Nb into the matrix does not affect to a great extent the presence of such terminal sites. Furthermore, both, AlF$_3$-OH$_{post}$ and Nb-AlF$_3$-OH$_{post}$ samples, show comparable ^{19}F MAS NMR data to their classical counterpart *HS*-AlF$_3$, suggesting likewise a high catalytic activity.
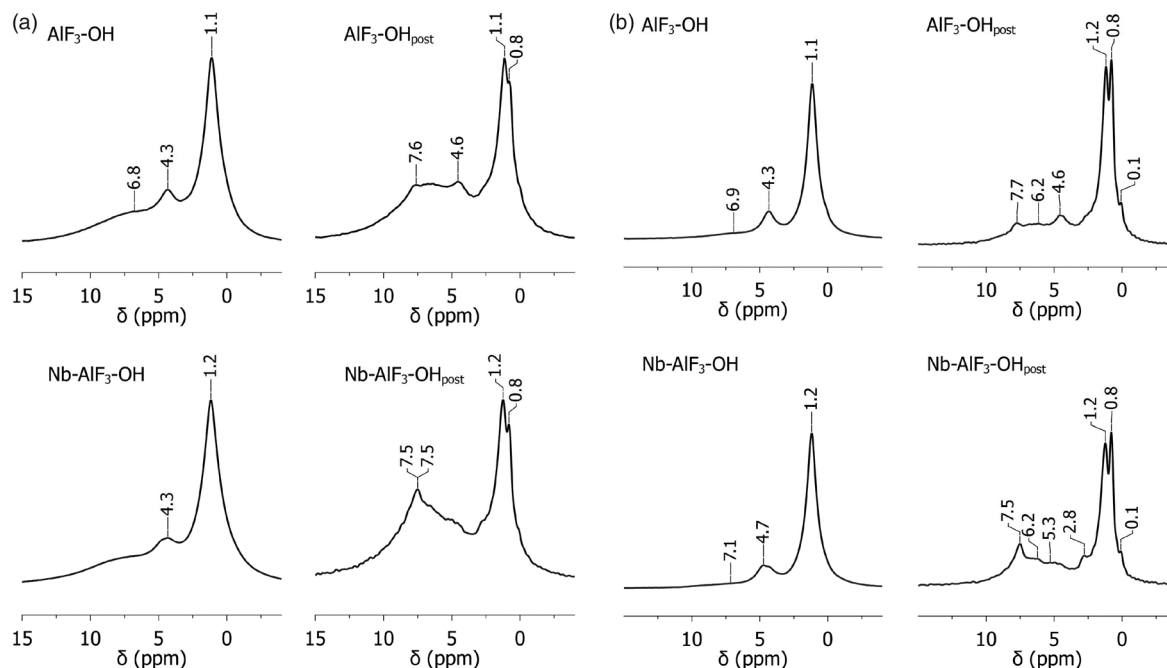
Fig. 8 (a) ^{1}H MAS NMR spectra for AlF$_3$-OH (up-left), AlF$_3$-OH$_{post}$ (up-right), Nb-AlF$_3$-OH (down-left) and Nb-AlF$_3$-OH$_{post}$ (down-right). All spectra were measured with a rotation frequency of 20 kHz, a recycle delay of 5 s, and an accumulation number of 256. (b) ^{1}H MAS spin-echo-rotor-synchronized NMR spectrum for Nb-AlF$_3$-OH (down-left) and Nb-AlF$_3$-OH$_{post}$ (down-right) and for AlF$_3$-OH (up-left) and AlF$_3$-OH$_{post}$ (up-right); ν_{rot} = 20 kHz, dipolar evolution time: 0.5 ms, ns = 256, p_1 = 3.8 μs.

Note, fluorine atoms generally do not exhibit different chemical shift when at an aluminium centre the neighbouring oxygen atom belongs to an hydroxide or to an isopropoxide moiety. Therefore both isopropoxide and hydroxide groups might be present in AlF$_3$-OH$_{post}$ and Nb-AlF$_3$-OH$_{post}$ since their signals are not distinguishable.

^{1}H MAS NMR spectroscopy. ^{1}H MAS NMR spectroscopy should provide information on hydrogen-containing moieties since according to elemental analysis, both AlF$_3$-OH and Nb-AlF$_3$-OH exhibit less than 2.6% hydrogen content. At first glance, the signals (see Fig. 8A) are all quite broad and are hard to separate from each other. Even the high rotation frequency used (20 kHz) is not enough to resolve such spectra, and obviously, a large number of different hydrogen containing moieties are present in all the samples.

The spectra of AlF$_3$-OH and Nb-AlF$_3$-OH exhibit a comparable pattern with signals at 1.2 ppm, 4.3 ppm and 6.8 ppm, with different intensities. The chemical shifts and relative intensities of these signals can be assigned to –O^{i}Pr groups, and even adsorbed isopropanol based on studies by König.[27,28] Bridging highly acidic–OH species, stemming from Al–OH units, should be revealed by a signal at approximately 7.9 ppm according to Scholz *et al.*[29] In the present case, the signals are too broad and they would cover such a signal; therefore, a definite conclusion cannot be drawn. It is conceivable that AlF$_3$-OH and Nb-AlF$_3$-OH do possess bridging –OH groups, but the experimental conditions used to obtain the spectra do not allow to identify them unequivocally.

For AlF$_3$-OH$_{post}$ and Nb-AlF$_3$-OH$_{post}$, the spectra reveal again similar signal patterns, indicating that the addition of Nb does not modify to a great extent the structure of AlF$_3$-OH$_{post}$. Narrow signals appear at lower chemical shifts, 0.8 and 1.2 ppm, corresponding to methyl groups of the isopropoxide groups still unreacted. The signals at 2.8–5.3 ppm can be assigned to the CH groups. Between 4 and 10 ppm, a broad shoulder appears in both spectra, with slightly higher intensity at 7.5 ppm. Thus, at 7.5 ppm Nb-AlF$_3$-OH$_{post}$ exhibits a more intense signal than AlF$_3$-OH$_{post}$, and this might be an indication for a larger number of bridging –OH species. Literature data for zeolites assign very strong OH bridging groups to a signal at 7.7 ppm and OH terminal groups bound at aluminium to a signal at 0.8 ppm.[30]

The broad shoulders at high chemical shift values, characterized by peaks at 7.7 and 7.5 ppm, for AlF$_3$-OH$_{post}$ and Nb-AlF$_3$-OH$_{post}$, respectively, show increased intensity when compared to AlF$_3$-OH and Nb-AlF$_3$-OH. They arise from bridging OH groups and account for the Brønsted acidity that these catalysts possess. The data observed for these post-fluorinated phases can be understood by comparing it to previous work on fluoride-alkoxide phases.[31] There, the addition of small amounts of water in the course of the fluorolytic sol–gel synthesis of *HS*-AlF$_3$ increased the intensity of the shoulders between 4 and 10 ppm, too. A ^{1}H MAS NMR spectrum of an *HS*-AlF$_3$ xerogel shows an intensity ratio of 6 : 1 : 1 for the signals observed at 1.2 ppm, 4.3 ppm and 7 ppm; but this ratio changes with the addition of

water, due to an increase in the number of bridging OH groups.

Fig. 8B depicts the ^{1}H MAS spin-echo-rotor-synchronized NMR spectra. Comparisons in intensity between different solids are not possible anymore, since the environment of each proton, and its relaxation, cannot be predicted or quantified. These experiments, however, confirm what has been observed previously in the ^{1}H MAS NMR spectra, and now signals for the different proton species are properly distinguishable. The spectra of AlF$_3$-OH and Nb-AlF$_3$-OH are quite similar (Fig. 8B, left side). Signals at approximately 1, 4 and 7 ppm can be identified, but overall they are still distinctively broad. Note that broad lines due to bridging OH species show a lower intensity due to the dipolar evolution time in the echo experiment (*cf.* Fig. 8B and caption).

Many different signals appear in the echo experiment in the post-fluorinated phases AlF$_3$-OH$_{post}$ and Nb-AlF$_3$-OH$_{post}$, which before were not distinguishable under the broad shoulder from 4 to 10 ppm. This is an indication that there are many different types of proton environments in the solid, which again stresses the presence of several types of OH groups with different identities.

Acid sites characterization

NH$_3$-TPD. To determine the overall number of acid sites and the strength distribution, ammonia TPD experiments were carried out. Table 1 shows the total number of acid sites and data normalized by BET surface area for each catalyst studied, as determined by quantification of the desorbed ammonia. Remarkably, most catalysts exhibit an increased absolute number of acid sites when compared to the *HS*-AlF$_3$ or the Nb-AlF$_{3-post}$ doped variant, with the exception of AlF$_3$-OH, which has a similar value. However, this is mainly due to the evidently larger surface area but becomes negligible when comparing the specific site density (number of acid sites per m^2). When comparing the precursor and post-fluorinated catalysts, the postfluorination increases not only the total number of acid sites but also the specific acid sites per surface area by a factor of two due to the reduction in BET surface area. These

values are even higher than those of *HS*-AlF$_3$, meaning that the fluorination with aqueous HF is a successful way to introduce a high density of acid sites in the porous matrix of the catalysts.

The profiles obtained during the thermal desorption of ammonia are depicted in Fig. 9. All the samples show a different acid strength distribution, from medium-strong (desorption up to *ca.* 400 °C) to very strong acid sites (above 400 °C). In the case of AlF$_3$-OH, the TPD exhibits a broad peak from 150 °C to 420 °C, and a narrower one between 420 °C and 500 °C, both with similar intensities. The post-fluorinated variant, AlF$_3$-OH$_{post}$, shows the same general behaviour, with additional desorption peaks. In the case of the Nb-doped catalysts, the two catalysts show different shape in the desorption. Nb-AlF$_3$-OH is more pronounced structured and shows four different desorption peaks, two of them corresponding to very strong acid sites, whereas Nb-AlF$_3$-OH$_{post}$ exhibits only two peaks, one characteristic for medium-strength sites and a smaller one for very strong sites at 500 °C. This suggests that the postfluorination step for the Nb-doped catalyst does not produce an increase in the total number of acid sites (see Table 1), but medium and strong sites seem to be converted into weaker and very strong sites.

Pyridine-FT-IR-PAS. Pyridine coordinatively binds to Lewis acid sites (Lpy) through the lone pair of electrons, whereas at Brønsted acid sites the aromatic nitrogen of the ring can be protonated (BpyH$^+$).[32–34] The vibrations of the pyridine ring can be assigned to Lpy (1445 and 1490 cm^{-1}) and to BpyH$^+$ (1490 and 1545 cm^{-1}) in the spectral window of 1400 to 1600 cm^{-1}. If both types of acid sites are present in a solid catalyst, the IR spectra will show three bands, two of which can be assigned exclusively to Lpy (at 1445 cm^{-1}) and to BpyH$^+$ (at 1545 cm^{-1}), and a third one which is an overlap of the bands of both Lpy and BpyH$^+$. Experimentally the method of choice is photoacoustic spectroscopy, because powders or opaque samples can be directly measured;[32,35] moreover it permits rapid measurements.

Fig. 10 shows the spectra obtained after pyridine adsorption. All four catalysts exhibit both kinds of acid sites, Lewis and Brønsted, as indicated by the presence of three bands.
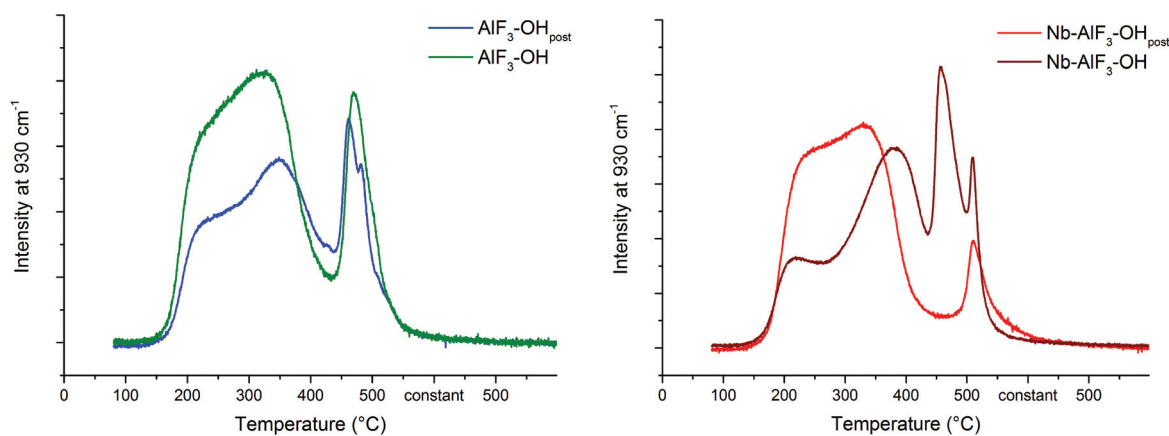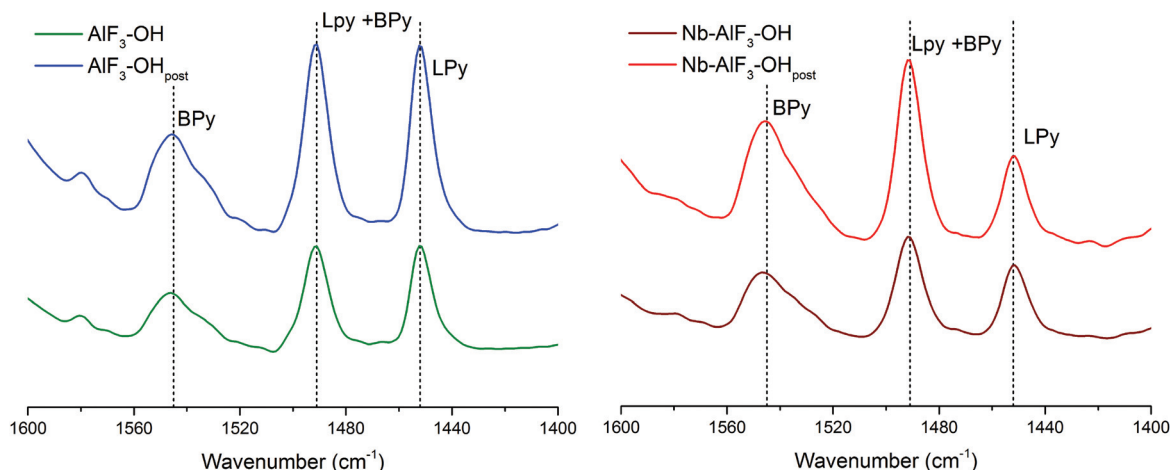

Fig. 9 NH$_3$ TPD profiles for AlF$_3$-OH and AlF$_3$-OH$_{post}$ (left) and Nb-AlF$_3$-OH and Nb-AlF$_3$-OH$_{post}$ (right).

Fig. 10 FT-IR-photoacoustic measurement after pyridine adsorption for AlF_3-OH and AlF_3-OH_{post} (left) and Nb-AlF_3-OH and Nb-AlF_3-OH_{post} (right). Signals corresponding to Lewis acid site-bounded pyridine (LPy) and to Brønsted acid site-bounded pyridine (BPy).

Noticeably, the addition of Nb causes an increase of Brønsted acid sites, observed in the change of the ratio of Lpy to BpyH$^+$ when compared to both AlF_3-OH_{post} and AlF_3-OH. Quantification is not recommended due to the too low sensitivity of this method, but apparently, Nb-AlF_3-OH_{post} and Nb-AlF_3-OH possess more Brønsted than Lewis acid sites. AlF_3-OH_{post} and AlF_3-OH exhibit a more intense signal for Lewis acid sites, however, Brønsted acid sites are still present but minor. It is remarkable that the postfluorination step seems not to have a significant effect on the ratio of Brønsted vs. Lewis acid site distribution, and the higher intensities of the peaks for AlF_3-OH_{post} may indicate an increase of the overall number of acid sites in the sample. Even for Nb-AlF_3-OH_{post}, the Brønsted acid sites increased just slightly.

Taking together the NH_3-TPD and the Py-FTIR results for AlF_3-OH_{post} and AlF_3-OH there seems no significant effect of the post fluorination step on the identity of acid sites (Brønsted vs. Lewis) and the site strength distribution. On the contrary, in the case of the niobium-containing catalysts, the ratio of the type of acid sites seems also to be unchanged but the site strength distribution changed as a result of post-fluorination. Moreover, considering the two peaks of the Nb-AlF_3-OH sample at 500 °C and above 500 °C in the NH_3-TPD measurements, it implies that the post-fluorinated sample Nb-AlF_3-OH_{post} even lost some very strong acid sites. The observed differences between both pairs of catalysts (before and after post-fluorination) are not entirely clear. First of all, perhaps they are due to the presence of both Nb–F and Nb–OH species on the surface of the catalyst. The latter species, which originate from the aqueous media used to fluorinate the alkoxides, is responsible for the Brønsted acidity, whereas the Nb–F and the majority of the Al–F sites in the solid account for Lewis acid sites. The doping with Nb centres to the AlF_3-catalyst obviously generates a larger number of terminal OH species as compared to the undoped one. After post-fluorination, most of those terminal Al–OH species in Nb-AlF_3-OH transfer into Al–F units and thus in Nb-AlF_3-OH_{post} strong sites are converted

into very strong acid sites. Likewise, Al–OH groups in AlF_3-OH are converted into strong Lewis acid sites (Al–F). There is no remarkable difference in the NH_3-TPD profile because Brønsted acid sites are converted into Lewis acid sites of apparently similar strength.

As to the higher portion of Brønsted sites in all the Nb-AlF_3-OH_{post} samples, a reasonable explanation is the fact that the bonding energy of Nb–O (726 kJ mol^{-1}) is higher than that of Nb–F bonds (452 kJ mol^{-1}) whereas Al–O bonds (501 kJ mol^{-1}) are significantly weaker than Al–F bonds (665 kJ mol^{-1}).[36] Thus, Nb–OH and/or Nb–OR groups that originate from the synthetic approach are quite more difficult to postfluorinate as compared to Al–OH and/or Al–OR groups. This also implies that, once fluorinated, Nb–F bonds are less stable than Al–F bonds against the attack of water, and thus can undergo hydrolysis more easily.[36] This data thus explain that the observed higher amount of Brønsted sites in all the Nb samples is reasonable.

Catalytic reactions

Dismutation of $CHClF_2$. One of the three reactions that were chosen in order to probe the strength and kind of acid surface sites (Lewis vs. Brønsted) of these new catalysts is the dismutation of chlorodifluoromethane, HCFC-22 (see Fig. 3a). HCFC-22 is a greenhouse gas long time used as a refrigerant in the past but still the intermediate for polytetrafluoroethylene (PTFE) production and is an excellent smooth fluorinating agent for preparing the post-fluorinated catalysts. An advantageous side-effect is that during the course of the postfluorination the degree of catalytic dismutation of HCFC-22 at different temperatures can be used to monitor the formation of catalytic active Lewis sites. After two hours heterogeneous reaction between the catalyst precursor and HCFC-22 full catalytic dismutation activity had been achieved at already 200 °C for the formation of Nb-AlF_3-OH_{post} and at 240 °C for AlF_3-OH_{post}. Then the reactor was cooled down and the dismutation conversion measured again at room temperature: this value is

in itself an excellent indication of the presence of strong Lewis acid sites.

Table 2 illustrates the values obtained for these two post-fluorinated catalysts, along with those for *HS*-AlF$_3$ and Nb-AlF$_{3\text{-post}}$, which were in the course of the fluorolytic sol–gel synthesis fluorinated with a-HF in isopropanol. All catalysts exhibit outstanding catalytic performance at room temperature, making AlF$_3$-OH$_{post}$ and Nb-AlF$_3$-OH$_{post}$ comparable in activity with *HS*-AlF$_3$. The Nb-containing catalyst already shows full conversion at 200 °C, indicating an advanced creation of strong Lewis surface sites in the doped catalyst when compared with the un-doped *HS*-AlF$_3$ catalyst, just as in the case of *HS*-AlF$_3$ when compared with Nb-AlF$_{3\text{-post}}$.

Isomerization of 1,2-dibromohexafluoropropane. Isomerization of dibromopolyfluoroalkanes was tested by Petrov *et al.* in

order to probe the extremely strong Lewis acidity of aluminium chlorofluoride.[37] Even with SbF$_5$, considered classically as the strongest Lewis acid at all – now surpassed by various molecular Lewis superacids,[38–40] only at 80 °C and 2 h reaction time conversion above 90% is achieved. This reaction occurs at room temperature only in the presence of very strong Lewis acid sites and can be considered as a benchmark reaction.[2] With AlCl$_3$ no reaction takes place at room temperature and only after 3 days at 150 °C, 74% conversion is observed.[41] Therefore, reactivity at room temperature was tested (see Fig. 3b and Table 3). In the case of AlF$_3$-OH and Nb-AlF$_3$-OH, no reactivity was observed. On the other hand, both AlF$_3$-OH$_{post}$ and Nb-AlF$_3$-OH$_{post}$ turned out to be excellent catalysts, exhibiting more than 90% conversion of 1,2-dibromohexafluoropropane to 2,2-dibromohexafluoropropane after only 2 hours at room temperature. These results confirm the observation that the postfluorination step is crucial in creating very strong acid sites by transforming the aluminium alkoxide groups that still remain inside the AlF$_3$-phases after their fluorolytic sol–gel preparation into more reactive aluminium fluoride ones. Remarkably, it is the first time that a AlF$_3$ phase with a significant content of Brønsted acidic surface sites exhibits very strong Lewis sites that fully catalyse the isomerization of 1,2-dibromohexafluoropropane.

For comparison, the above-mentioned catalysts, prepared *via* fluorination with anhydrous HF in isopropanol, are also included in Table 3. Nb-AlF$_{3\text{-post}}$ shows less than 20% conversion in this particular reaction.[17] This is in agreement with the conclusions made at that time, since for the Nb-doped samples a direct relationship between the decrease of reactivity and higher amount of Nb centres in the catalyst samples was observed. However, the aqueous synthesis route obviously alters the material in such a way that the AlF$_3$-based catalysts obtained – even doped by Nb – display very strong Lewis acid sites, thus affording full conversion for this reaction at room temperature. A plausible explanation for this difference between Nb-AlF$_{3-post}$ and Nb-AlF$_3$-OH$_{post}$ originates from the application of HF$_{aq}$, which leads to a higher degree of fluorination during the sol–gel approach, due to the higher acidity.

Cyclization of citronellal. Pyridine FTIR spectroscopy clearly evidenced the presence of both, Lewis and Brønsted acid sites,

Table 2 Dismutation of chlorodifluoromethane during post fluorination step

Entry	Catalyst	Conversion at 200 °C [a] [%]	Conversion at 240 °C [a] [%]	Conversion at 30 °C [a] [%]
1	*HS*-AlF$_3$ [c]	2	96	99
2	Nb-AlF$_{3\text{-post}}$ [c]	97	[b]	99
3	AlF$_3$-OH$_{post}$	1	99	98
4	Nb-AlF$_3$-OH$_{post}$	97	[b]	99

[a] Calculated relatively by integration of peak area in its respective chromatogram. [b] Reaction performed until 200 °C. [c] From ref. 17.

Table 3 Isomerization of 1,2-dibromohexafluoropropane to 2,2-dibromohexafluoropropane[a]

Entry	Catalyst	Conversion [%]
1	*HS*-AlF$_3$ [b]	99
2	Nb-AlF$_{3\text{-post}}$ [b]	15
3	AlF$_3$-OH$_{post}$	99
4	AlF$_3$-OH	0
5	Nb-AlF$_3$-OH$_{post}$	95
6	Nb-AlF$_3$-OH	0

[a] Reaction conditions: 2 h, 25 °C. Conversion calculated from integration of ^{19}F NMR. [b] See ref. 17.

Table 4 Cyclization of citronellal to isopulegol[a]

Entry	Catalyst	Conversion of citronellal [%]	Total yield to isopulegols[b] [%]	Selectivity to isopulegol (A)[c] [%]	Yield of isopulegol (A) [%]
1	*HS*-AlF$_3$ [d]	91.7	55.8	51.2	28.6
2	Nb-AlF$_{3\text{-post}}$ [d]	98.8	74.8	48.7	36.4
3	AlF$_3$-OH$_{post}$	83.5	40.6	50.6	20.6
4	AlF$_3$-OH	95.4	48.1	52.2	25.1
5	Nb-AlF$_3$-OH$_{post}$	99.4	58.0	49.6	28.8
6	Nb-AlF$_3$-OH	99.4	46.9	50.7	23.8

[a] Reaction conditions: 6 h, 80 °C, 600 rpm; 3 mL toluene, 0.3 mL citronellal and 0.15 mL undecane as internal standard. All the values were calculated *via* GC/FID using a calibration curve for citronellal and the retention times were compared to the literature.[15] A blank reaction without a catalyst was carried out. Conversion of citronellal was quantified (4.7%) and the given values were corrected accordingly. [b] Calculated based on the initial amount of citronellal, for all four possible isomers. [c] Selectivity to isopulegol (A) over the other three isomers. [d] See ref. 17.

especially in the Nb-doped HS-AlF$_3$. An interesting reaction to test the bi-acidic character of catalysts is the cyclization of citronellal. This reaction is considered to proceed only in the presence of a catalyst bearing both Lewis and Brønsted acid sites and has been studied as a model acid-catalyzed reaction by Chuah et al., since it is also of interest for the industrial production of menthol.[42] For a successful conversion and selectivity to obtain the desired product isopulegol and their corresponding isomers, two steps need to take place: the isomerization of the double bond followed by protonation of the oxygen of the ketone group and ring closure. This mechanism requires not only the presence of both Lewis and Brønsted acid sites in the catalyst but also a distribution of those sites in a neighbouring position.[42,43]

Consequently, the cyclization of citronellal (depicted in Fig. 3c) was used to probe the presence of both kinds of acid sites and to test all the four catalysts studied here. The results are summarized in Table 4. Additional values are included for comparison (HS-AlF$_3$ and Nb-AlF$_{3\text{-post}}$). All catalysts show excellent conversions for citronellal (more than 83%), with a slight improvement for the Nb-doped ones (up to 99%). The total yield for all the isopulegol isomers is higher than 40%, and in the case of Nb-AlF$_3$-OH$_{post}$, the best result can be obtained, with a 58% yield. The selectivity to isopulegol (A) over the other three isomers is similar for all the catalysts.

The addition of Nb centres seems to be a factor that enhances conversion and total yield, and its effect is more pronounced when the catalysts are post-fluorinated (e.g. comparing AlF$_3$-OH$_{post}$ vs. Nb-AlF$_3$-OH$_{post}$). Nb-AlF$_3$-OH$_{post}$ shows the best performance, with the highest conversion of citronellal and a very good overall yield for all isopulegol isomers. For AlF$_3$-OH and AlF$_3$-OH$_{post}$, the postfluorination step leads to a worsening of the catalytic performance. Two hypotheses can be provided in order to rationalize this effect. A first possible reason might be that the Brønsted acid sites which are needed for this reaction have been drastically reduced in the course of post-fluorination in AlF$_3$-OH$_{post}$. Due to the strong difference in the binding energies between Al–OH and Al–F bonds, the majority of Al–OH bonds (which account for the Brønsted acidity) are converted into Al–F bonds (which account for the Lewis acidity). Thus, conversion and selectivity towards isopulegols decrease. The situation is different in case of the Nb-doped catalysts. Nb-AlF$_3$-OH$_{post}$ and Nb-AlF$_3$-OH, contrary to their undoped variants, do still possess a higher proportion of Brønsted acid sites originating from Nb–OH surface sites. Additionally, it seems that OH-groups bound at Nb-sites do not interfere that much with Lewis Al-surface sites as Al–OH groups at the same Al-sites do.

Conclusion

In this paper we present a new, alternative and effective approach to prepare highly acidic aluminium fluoride phases. Such AlF$_3$-phases, after the postfluorination treatment, exhibit an extremely high catalytic activity in reactions such as the dis-

mutation of CHClF$_2$ and isomerization of 1,2-dibromohexafluoropropane. A remarkable difference from the already known HS-AlF$_3$ is that the use of HF$_{aq}$ permits to obtain a bi-acidic catalyst, where very strong Lewis acid sites coexist with Brønsted acid sites. The Nb-doped aluminium fluoride system presented here possess very strong Lewis acid sites, alongside Nb-OH groups accounting for Brønsted acid sites. Remarkably, the presence of Nb allows the introduction of OH groups which are preserved even after the post-fluorination treatment and do not affect the high strength of the Lewis acidic Al sites.

Conflicts of interest

There are no conflicts to declare.

Acknowledgements

References

1 G. Busca, *Heterogeneous Catalytic Materials: Solid State Chemistry, Surface Chemistry and Catalytic Behaviour*, Elsevier B.V., 2014.

2 T. Krahl and E. Kemnitz, *Catal. Sci. Technol.*, 2017, **7**, 773–796.

3 E. Kemnitz, U. Groß, S. Rüdiger and C. S. Shekar, *Angew. Chem., Int. Ed.*, 2003, **42**, 4251–4254.

4 S. Rüdiger and E. Kemnitz, *Dalton Trans.*, 2008, **9226**, 1117.

5 E. Kemnitz, *Catal. Sci. Technol.*, 2015, **5**, 786–806.

6 G. Scholz, S. Brehme, M. Balski, R. König and E. Kemnitz, *Solid State Sci.*, 2010, **12**, 1500–1506.

7 D. Dambournet, A. Demourgues, C. Martineau, S. Pechev, J. Lhoste, J. Majimel, A. Vimont, J. C. Lavalley, C. Legein, J. Y. Buzaré, F. Fayon and A. Tressaud, *Chem. Mater.*, 2008, **20**, 1459–1469.

8 D. Dambournet, A. Demourgues, C. Martineau, E. Durand, J. Majimel, A. Vimont, H. Leclerc, J.-C. Lavalley, M. Daturi, C. Legein, J.-Y. Buzaré, F. Fayon and A. Tressaud, *J. Mater. Chem.*, 2008, **18**, 2483–2492.

9 C. Stosiek, G. Scholz, G. Eltanany, R. Bertram and E. Kemnitz, *Chem. Mater.*, 2008, **20**, 5687–5697.

10 F. Hemmann, G. Scholz, K. Scheurell, E. Kemnitz and C. Jaeger, *J. Phys. Chem. C*, 2012, **116**, 10580–10585.

11 F. Hemmann, I. Agirrezabal-Telleria, C. Jaeger and E. Kemnitz, *RSC Adv.*, 2015, **5**, 89659–89668.

12 C. Stosiek, G. Scholz, S. L. M. Schroeder and E. Kemnitz, *Chem. Mater.*, 2010, **22**, 2347–2356.

13 I. Agirrezabal-Telleria, F. Hemmann, C. Jäger, P. L. Arias and E. Kemnitz, *J. Catal.*, 2013, **305**, 81–91.

14 F. Hemmann, C. Jaeger and E. Kemnitz, *RSC Adv.*, 2014, **4**, 56900–56909.

15 K. Teinz, PhD thesis, Humboldt Universität zu Berlin, 2012.

16 C. L. Bailey, S. Mukhopadhyay, A. Wander, B. G. Searle and N. M. Harrison, *J. Phys. Chem. C*, 2009, **113**, 4976–4983.

17 C. P. Marshall, T. Braun and E. Kemnitz, *Catal. Sci. Technol.*, 2018, **8**, 3151–3159.

18 D. G. Cory and W. M. Ritchey, *J. Magn. Reson.*, 1988, **80**, 128–132.

19 S. Rüdiger, G. Eltanany, U. Groß and E. Kemnitz, *J. Sol-Gel Sci. Technol.*, 2007, **41**, 299–311.

20 S. K. Rüdiger, U. Groß, M. Feist, H. A. Prescott, S. C. Shekar, S. I. Troyanov and E. Kemnitz, *J. Mater. Chem.*, 2005, **15**, 588.

21 T. Krahl, A. Vimont, G. Eltanany, M. Daturi and E. Kemnitz, *J. Phys. Chem. C*, 2007, **111**, 18317–18325.

22 M. Thommes, K. Kaneko, A. V. Neimark, J. P. Olivier, F. Rodriguez-Reinoso, J. Rouquerol and K. S. W. Sing, *Pure Appl. Chem.*, 2015, **87**, 1051–1069.

23 G. Leofanti, M. Padovan, G. Tozzola and B. Venturelli, *Catal. Today*, 1998, **41**, 207–219.

24 R. König, G. Scholz, A. Pawlik, C. Jäger, B. Van Rossum, H. Oschkinat and E. Kemnitz, *J. Phys. Chem. C*, 2008, **112**, 15708–15720.

25 R. König, G. Scholz, A. Pawlik, C. Jager, B. Van Rossum and E. Kemnitz, *J. Phys. Chem. C*, 2009, **113**, 15576–15585.

26 T. Krahl, R. Stösser, E. Kemnitz, G. Scholz, M. Feist, G. Silly and J.-Y. Buzaré, *Inorg. Chem.*, 2003, **42**, 6474–6483.

27 R. König, G. Scholz, R. Bertram and E. Kemnitz, *J. Fluor. Chem.*, 2008, **129**, 598–606.

28 R. König, G. Scholz and E. Kemnitz, *J. Phys. Chem. C*, 2009, **113**, 6426–6438.

29 G. Scholz, S. Brehme, R. König, D. Heidemann and E. Kemnitz, *J. Phys. Chem. C*, 2010, **114**, 10535–10543.

30 Y. Jiang, J. Huang, W. Dai and M. Hunger, *Solid State Nucl. Magn. Reson.*, 2011, **39**, 116–141.

31 R. König, G. Scholz and E. Kemnitz, *J. Sol-Gel Sci. Technol.*, 2010, **56**, 145–156.

32 J. Ryczkowski, *Catal. Today*, 2001, **68**, 263–381.

33 M. Tamura, K. Shimizu and A. Satsuma, *Appl. Catal., A*, 2012, **433–434**, 135–145.

34 M. C. Kung and H. H. Kung, *Catal. Rev.*, 1985, **27**, 425–460.

35 A. Rosencwaig and A. Gersho, *J. Appl. Phys.*, 1976, **47**, 64–69.

36 Y.-R. Luo, *Comprehensive Handbook of Chemical Bond Energies*, CRC Press Inc - M.U.A., 1st edn, 2007.

37 V. A. Petrov, C. G. Krespan and B. E. Smart, *J. Fluor. Chem.*, 1998, **89**, 125–130.

38 L. O. Müller, D. Himmel, J. Stauffer, G. Steinfeld, J. Slattery, G. Santiso-Quinones, V. Brecht and I. Krossing, *Angew. Chem., Int. Ed.*, 2008, 7659–7663.

39 J. F. Kögel, D. A. Sorokin, A. Khvorost, M. Scott, K. Harms, D. Himmel, I. Krossing and J. Sundermeyer, *Chem. Sci.*, 2018, **9**, 245–253.

40 A. Wiesner, T. W. Gries, S. Steinhauer, H. Beckers and S. Riedel, *Angew. Chem., Int. Ed.*, 2017, **56**, 8263–8266.

41 P. A. Morken and D. J. Burton, *J. Org. Chem.*, 1993, **58**, 1167–1172.

42 G. K. Chuah, S. H. Liu, S. Jaenicke and L. J. Harrison, *J. Catal.*, 2001, **200**, 352–359.

43 Z. Yongzhong, N. Yuntong, S. Jaenicke and G. K. Chuah, *J. Catal.*, 2005, **229**, 404–413.